

Quinones as Electron Acceptors. X-Ray Structures, Spectral (EPR, UV–vis) Characteristics and Electron-Transfer Reactivities of Their Reduced Anion Radicals as Separated vs Contact Ion Pairs

Jian-Ming Lü, Sergiy V. Rosokha, Ivan S. Neretin, and Jay K. Kochi*

Contribution from the Department of Chemistry, University of Houston, Houston, Texas 77204

Received September 12, 2006; E-mail: jkochi@UH.edu

Abstract: Successful isolation of a series of pure (crystalline) salts of labile quinone anion radicals suitable for X-ray crystallographic analysis allows for the first time their rigorous structural distinction as “separated” ion pairs (SIPs) vs “contact” ion pairs (CIPs). The quantitative evaluation of the precise changes in the geometries of these quinones (**Q**) upon one-electron reduction to afford the anion radical (**Q^{•-}**) is viewed relative to the corresponding (two-electron) reduction to the hydroquinone (**H₂Q**) via the Pauling bond-length/bond-order paradigm. Structural consequences between such separated and contact ion pairs as defined in the solid state with those extant in solution are explored in the context of their spectral (EPR, UV–vis) properties and isomerization of tightly bound CIPs. Moreover, the SIP/CIP dichotomy is also examined in intermolecular interactions for rapid (self-exchange) electron transfer between **Q^{•-}** and **Q** with second-order rate constants of $k_{ET} \approx 10^8 \text{ M}^{-1} \text{ s}^{-1}$, together with the spectral observation of the paramagnetic intermediates [**Q, Q^{•-}**] leading to 1:1 adducts, as established by X-ray crystallography.

Introduction

Quinones (**Q**) are ubiquitous in nature owing to their propensity to form various odd-electron intermediates in different types of biochemical (energy) processes.^{1,2} Although a wide number of quinones are indeed known and precisely identified by X-ray crystallographic analysis,³ there is a singular dearth of precise structural and spectroscopic information about the pure quinone anion radical (**Q^{•-}**) itself as the corresponding one-electron reduction product.⁴ No doubt, a large part of the difficulty resides in the tenuous effects of the counterion in ion pairing, especially as the associated cation modulates the local structure, the electronic transition, and the stability/reactivity of such an anionic entity.^{5,6} In this regard, the numerous

computational studies of reduced quinones that are extant^{7–9} must be recognized relative to the much needed experimental reference points for ion-pairing effects.

Ionic atmospheres that are characteristic of many biochemical systems¹⁰ imply the significant role of ion-pair formation in redox processes taking place in such environments. Moreover, the drastic effects of ion pairing on the kinetics and thermodynamics of (artificial) redox reactions of quinone derivatives,^{5,11} as well as its effect on the counterion-controlled intramolecular charge redistribution within unsymmetrical anion radicals, have been experimentally documented.^{6,12,13} Thus, earlier EPR studies

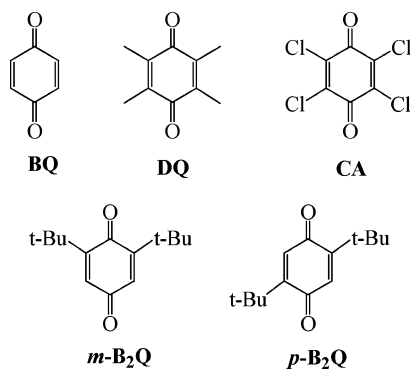
- (1) *The Chemistry of Quinonoid Compounds*; Patai, S., Ed.; Wiley & Sons: New-York, 1974.
- (2) *Function of Quinones in Energy-Conserving Systems*; Trumpower B. L., Ed.; Academic Press: New York, 1986. (b) Blankenship, R. E. *Molecular Mechanism of Photosynthesis*; Blackwell Science: Cambridge, MA, 2001.
- (3) (a) van Bolhuis, F.; Kiers, C. T. *Acta Crystallogr., Sect. B* **1978**, *34*, 1015. (b) Rabinovich, D.; Schmidt, G. M.; Ubel, E. J. *Chem. Soc. B* **1967**, 131. (c) Aleksandrov, G. G.; Struchkov, Yu. T.; Kalinin, D. I.; Neigauz, M. G. *Zh. Strukt. Khim.* **1973**, *14*, 852.
- (4) For the structures of cyano- and/or chloro-substituted *p*-benzoquinone acceptors and their anion radicals, see: (a) Ganesan, V.; Rosokha, S. V.; Kochi, J. K. *J. Am. Chem. Soc.* **2003**, *125*, 2559. (b) For the structure of the anion radical of tetraphenyl-*p*-benzoquinone, see: Bock, H.; John, A.; Nather, C. *Chem. Commun.* **1994**, 1939.
- (5) Szwarc, M., Ed. *Ions and Ion Pairs in Organic Reactions*; Wiley: New York, 1972; Vols. 1 and 2.
- (6) (a) Khakhar, M. P.; Prabhananda, B. S.; Das, M. R. *Chem. Phys.* **1966**, *45*, 2327. (b) Khakhar, M. P.; Prabhananda, B. S.; Das, M. R. *J. Am. Chem. Soc.* **1967**, *89*, 3100. (c) Konishi, S.; Niizuma, S.; Kokubun, H. *Chem. Phys. Lett.* **1980**, *71*, 164. (d) Flimt, N. J.; Tabner, B. J. *J. Chem. Soc., Perkin Trans. 2* **1984**, 569. (e) Sueishi, Y.; Kasahara, M.; Okawa, K.; Yamamoto, S. *Z. Phys. Chem.* **2004**, *218*, 1187. (f) Stevenson, G. R.; Alegria, A. E.; Block, A. McB. *J. Am. Chem. Soc.* **1975**, *97*, 4859.

- (7) (a) O'Malley, P. J. *J. Phys. Chem. A* **1997**, *101*, 6334. (b) Zhan, C.-G.; Chipman, D. M. *J. Phys. Chem. A* **1998**, *102*, 1230. (c) O'Malley, P. J. *J. Am. Chem. Soc.* **1998**, *120*, 5093. (d) Mohapatra, H.; Umaphathy, S. *J. Phys. Chem. A* **2002**, *106*, 4513. (e) Engstrom, M.; Vahtras, O.; Agren, H. *Chem. Phys.* **1999**, *243*, 263.
- (8) (a) Boesch, S. E.; Wheeler, R. A. *J. Phys. Chem. A* **1997**, *101*, 8351. (b) Wise, K. E.; Grafton, A. K.; Wheeler, R. A. *J. Phys. Chem. A* **1997**, *101*, 1160. (c) Grafton, A. K.; Wheeler, R. A. *J. Phys. Chem. A* **1997**, *101*, 7154. (d) Eriksson, L. A.; Himo, F.; Siegbahn, P. E. M.; Babcock, G. T. *J. Phys. Chem. A* **1997**, *101*, 9496. (e) Himo, F.; Babcock, G. T.; Eriksson, L. A. *J. Phys. Chem. A* **1999**, *103*, 3745. (f) Honda, Y.; Hada, M.; Ehara, M.; Nakatsuji, H. *J. Phys. Chem. A* **2002**, *106*, 3838.
- (9) (a) O'Malley, P. J. *J. Phys. Chem. A* **1998**, *102*, 248. (b) Kaupp, M.; Remenyi, C.; Vaara, J.; Malkina, O. L.; Malkin, V. G. *J. Am. Chem. Soc.* **2002**, *124*, 2709.
- (10) Bohinski, R. C. *Modern Concepts in Biochemistry*, 2nd ed.; Allyn and Bacon: Boston, 1976.
- (11) (a) Yuasa, J.; Suenobu, T.; Fukuzumi, S. *ChemPhysChem* **2006**, *7*, 942. (b) Yuasa, J.; Suenobu, T.; Fukuzumi, S. *J. Am. Chem. Soc.* **2003**, *125*, 12090. (c) Okamoto, K.; Imahori, H.; Fukuzumi, S. *J. Am. Chem. Soc.* **2003**, *125*, 7014. (d) Fukuzumi, S.; Ohkubo, K.; Okamoto, A. T. *J. Am. Chem. Soc.* **2002**, *124*, 14147. (e) Okamoto, K.; Ohkubo, K.; Kadish, K. M.; Fukuzumi, S. *J. Phys. Chem. A* **2004**, *108*, 10405.
- (12) (a) Oakes, J.; Symons, M. C. R.; Claxton, T. A. *J. Am. Chem. Soc.* **1971**, *93*, 3769. (b) Chen, K. S.; Hirota, N. *J. Phys. Chem.* **1978**, *82*, 1133.
- (13) (a) Echegoyen, L.; Nieves, I.; Stevenson, G. R. *J. Phys. Chem.* **1982**, *86*, 1611. (b) Kabaya, S.; Luz, Z.; Goldfarb, D. *J. Am. Chem. Soc.* **1994**, *116*, 5805.

led to the conclusion that (i) solutions of these anion radicals contain both ion-paired and “free” or solvent-separated species; (ii) the inequivalent proton hyperfine splittings of the “ion-paired” anion radicals are indicative of two species, the facile interchange between which is modulated by intramolecular counterion migration, as deduced by temperature-dependent (selective) linebroadening behavior;^{6,12,13} and (iii) the coexistence of the quinone anion radical ($\text{Q}^{\bullet-}$) with its neutral parent (Q) leads to rapid self-exchange electron transfer with second-order rate constants of 10^7 to $10^8 \text{ M}^{-1} \text{ s}^{-1}$, as evaluated by dynamic EPR line broadening behavior.^{14,15}

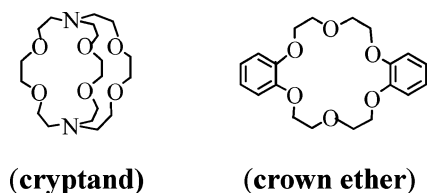
Owing to the absence of definitive structural information of $\text{Q}^{\bullet-}$ either as the free anion (equivalent to the “separated” salt: $\text{M}^+/\text{Q}^{\bullet-}$) or as the anion in close “contact” with its counter-cation ($\text{M}^+\text{Q}^{\bullet-}$),¹⁶ we initially focus on the preparation of pure crystalline salts suitable for X-ray crystallography of the graded series of quinone derivatives depicted in Chart 1.

Chart 1



The crystallographic distinction between the *contact* ion pair (CIP) and the *separated* ion pair (SIP) is then enforced by the use of polyether ligands (L) of the ligated potassium counterion as K(L)^+ . Thus our previous studies showed that when $\text{L} = [2,2,2]\text{cryptand}$ (Chart 2), the potassium cation, $\text{K}(\text{cryptand})^+$,

Chart 2



is completely encased by the three-dimensional ligand sufficient to isolate it from the anion radical as the SIP.^{17,18} As a result, the quinone anion radical in its interionic association with the cryptand-encapsulated K^+ counter-cation to form the SIP can

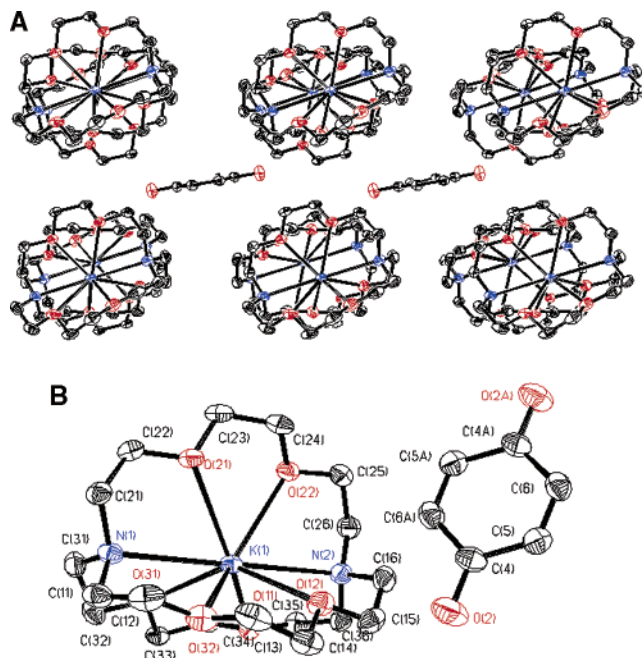


Figure 1. (A) Crystal lattice of the $\text{K}(\text{cryptand})^+\text{BQ}^{\bullet-}$ as polymorph I and (B) its ORTEP designation. For the contrasting structure of polymorph II, see Figure S1 in the Supporting Information.

be considered as an essentially “free” undisturbed anionic entity. On the other hand, the nesting of a potassium cation in the cavity of a two-dimensional crown ether (Chart 2) leaves an axial position accessible for direct (covalent) coordination of a quinonoid oxygen center, and the effects of such a tight binding will be symptomatic of the CIP sufficient to affect the structures and spectral properties of the quinone anion radical. Accordingly, in this study, we focus our attention on (1) isolating pure crystalline salts of the quinone anion radicals in Chart 1, with K(L)^+ , where $\text{L} = \text{cryptand}$ and crown ether in Chart 2 for X-ray crystallographic analysis; (2) relating their solid-state structures with those extant in solution; and (3) examining the effects of ion pairing on the various redox behaviors of these anion radicals.

Results and Discussion

I. Preparation and X-ray Analysis of Quinone Anion Radicals as Crystalline Salts of the Ligated Potassium Cation K(L)^+ . A. Separated Ion-Pair Structures with $\text{L} = [2,2,2]\text{-Cryptand}$. Potassium-mirror reduction of the parent *p*-benzoquinone (**BQ**) in the presence of $[2,2,2]\text{cryptand}$ results in the crystallization of two modifications of the 1:1 anion-radical salts according to eq 1:



which are hereinafter referred to as polymorphs I and II, the details of which are presented in the Experimental Section. The asymmetric unit cell of polymorph I with space group $P\bar{1}$ consists of individually distinct $\text{BQ}^{\bullet-}$ anions and $\text{K}(\text{cryptand})^+$ cations in which the crystal packing (Figure 1) is dominated by the highly encumbered potassium(cryptand) cations, with benzoquinone anion radicals positioned in the voids between them. Indeed, the well-separated cations and anions form their own stacking motif; the potassium–oxygen distances of 5.64 Å and of 6.17 Å (as well as the separation between potassium

- (14) (a) Layoff, T.; Miller, T.; Adams, R. N.; Fan, H.; Horsfield, A.; Proctor, W. *Nature* **1965**, *205*, 382. (b) Meisel, D.; Fessenden, R. W. *J. Am. Chem. Soc.* **1976**, *98*, 7505.
- (15) Fukuzumi, S.; Nakanishi, I.; Suenobu, T.; Kadish, K. M. *J. Am. Chem. Soc.* **1999**, *121*, 3468.
- (16) Our operational classification of the *contact* ion pair herein requires direct interionic contact between the positive and negative centers (within their van der Waals radii). By contrast, such a direct electrostatic interaction between cation/anion centers is modified in *separated* ion pairs by intervention of one or more solvent, ligand, etc.^{5,17}
- (17) (a) Davlieva, M. G.; Lu, J.-M.; Lindeman, S. V.; Kochi, J. K. *J. Am. Chem. Soc.* **2004**, *126*, 4557. (b) Lu, J.-M.; Rosokha, S. V.; Lindeman, S. V.; Neretin, I. S.; Kochi, J. K. *J. Am. Chem. Soc.* **2005**, *127*, 1797.
- (18) Rosokha, S. V.; Lu, J.-M.; Newton, M. D.; Kochi, J. K. *J. Am. Chem. Soc.* **2005**, *127*, 7411.

and the other atoms of benzoquinone) are significantly greater than the sum of their van der Waals radii.¹⁹

The unit cell of the polymorphic modification II of the $K(\text{cryptand})^+\text{BQ}^-$ salt consists of one potassium(cryptand) cation and one quinone anion radical (space group: $P2_1/n$) in which the cations and anions adopt an alternating pattern in the formation of stacks propagating along the c -axis (see packing diagram of II in Figure S1 in the Supporting Information). Furthermore, the separation of 5.33 Å between the potassium cation and the oxygen atom of the anion radical in polymorph II is slightly shorter than that in modification I. However, such a value is nonetheless much longer than the sum of their van der Waals radii and reemphasizes the fact that the benzoquinone moiety is well-separated from the counterion in polymorph II as well.

The X-ray analyses of crystalline salts formed upon alkali-metal reduction of the other acceptors from Chart 1 in the presence of [2,2,2]cryptand generally show similar anion/cation arrangements (see Figures S2–S5 in the Supporting Information). Most importantly, the use of the three-dimensional cryptand ligand ensures the significant separation of the anion-radical moiety from the alkali-metal counterions in all of these salts. For example, the permethylated quinone analogue **DQ** yields the 1:1 salt $K(\text{cryptand})^+\text{DQ}^-$ which crystallizes as the THF solvate in space group $P\bar{1}$ (see packing diagram in Figure S2), in which the potassium distances to the oxygen atoms of the benzoquinone anion radical are 6.63 and 5.71 Å.

The two sterically hindered quinones: $m\text{-B}_2\text{Q}$ and $p\text{-B}_2\text{Q}$ (with a pair of *tert*-butyl substituents as the meta and para isomers illustrated in Chart 1) also yield pure crystalline salts $K(\text{cryptand})^+m\text{-B}_2\text{Q}^-$ and $K(\text{cryptand})^+p\text{-B}_2\text{Q}^-$, respectively, in which the long potassium–oxygen separations of 6.30 and 6.74 Å in the salts underscore their separated ion-pair character (see Figures S3 and S4). Such an extended cation/anion distance is also observed in the corresponding sodium salts (prepared via sodium-mirror reduction) of chloranil anion radical $\text{Na}(\text{cryptand})^+\text{CA}^-$ (Figure S5) with a long Na–O separation of 5.25 Å.

B. Contact Ion-Pair Structures with L = Crown Ether. Potassium-mirror reduction of *p*-benzoquinone (**BQ**) in the presence of L = dibenzo-18-crown-6 (crown ether) results in pure 1:1 crystals of $K(\text{crown ether})^+\text{BQ}^-$ in which each potassium cation is equatorially coordinated by crown ether and axially coordinated (via oxygen) to benzoquinone anion radical (Figure 2A). The opposite axial position is also occupied by an oxygen from a second BQ^- ; the remaining carbonyl groups of both benzoquinones are in turn coordinated to potassium cations, which leads to the formation of the infinite anion/cation chains in Figure 2B. Importantly, the close proximity of the axial oxygens to potassium with the K–O bond lengths of 2.65 and 2.73 Å is indicative of contact ion pairs, and such bonding distances are characteristic for a variety of organic oxygen-containing anions with potassium counterions.²⁰ Notably, the

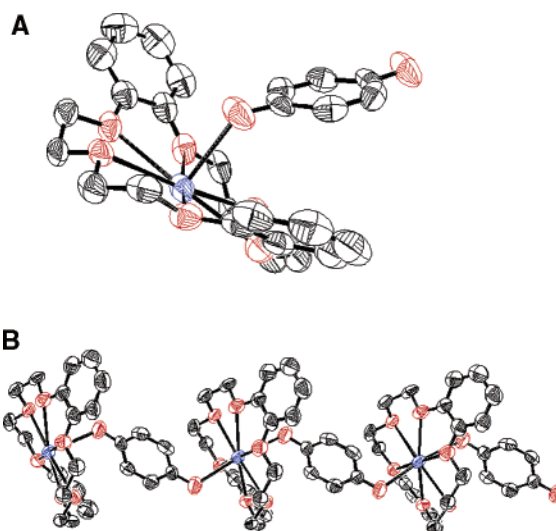


Figure 2. (A) ORTEP diagram of the 1:1 salt $K(\text{crown ether})^+\text{BQ}^-$ and (B) the interionic chain character in the crystal lattice.

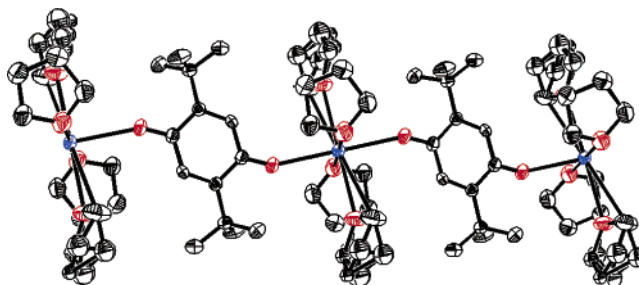


Figure 3. Fragment of the crystal lattice of $K(\text{THF})_4^+p\text{-B}_2\text{Q}^-$ showing the anion radical coordinated to two potassium counterions (ligated by four THF solvates) in an infinite chain.

cation locations deviate significantly from the benzoquinone plane, the angles between the K–O and O=C bonds being 117° and 111° and the C–C–O–K dihedral angles of 67° and 61° for the potassium coordinated at opposite ends of benzoquinone.

In the absence of either cryptand or crown ether, the potassium-mirror reduction of a quinone in THF leads to another type of contact ion-pair structure. For example, the di-*tert*-butyl-substituted $p\text{-B}_2\text{Q}$ yields pure crystalline salts with an overall stoichiometry of $K(\text{THF})_4^+p\text{-B}_2\text{Q}^-$ in which the unit cell consists of half the corresponding anion radical, half a potassium cation, and two THF solvates (space group: $P\bar{1}$). In this case, the oxygen atoms of the anion radical $p\text{-B}_2\text{Q}^-$ are coordinated to a pair of potassium cations, and the equatorial positions of each potassium cation are occupied by four THF solvates. As such, this contact ion pair forms a continuous chain propagating in the unit cell as shown in Figure 3. The geometric characteristics of the bonding between the carbonyl oxygens and potassium cations with the K–O separation of 2.62 Å are identical on both ends of the quinone moiety in $K(\text{THF})_4^+p\text{-B}_2\text{Q}^-$ (Figure 3) but are slightly shorter than those presented in the salt of the unsubstituted $K(\text{crown ether})^+\text{BQ}^-$. Furthermore, the out-of-plane angle between the K–O and O=C bonds is 150°, and the C–C–O–K dihedral angle is 44° (and this results in the cations lying somewhat closer to the quinone plane).

Potassium-mirror reduction of the unsymmetrically substituted acceptor $m\text{-B}_2\text{Q}$ in the presence of dibenzo-18-crown-6 results in the formation of crystals with the unit cell containing a single

(19) For the K–O contact, the sum of the van der Waals radii is 4.3 Å.

(20) For other examples of similar bonding of crown-ether-ligated potassium, see: (a) Caswell, L. R.; Hardcastle, J. E.; Jordan, T. A.; Alam, I.; McDowell, K. A.; Mahan, C. A.; Fronczek, F. R.; Gandour, R. D. *J. Inclusion Phenom. Macrocyclic Chem.* **1992**, *13*, 37. (b) Veya, P.; Floriani, C.; Chiesi-Villa, A.; Rizzoli, C. *Organometallics* **1994**, *13*, 214. (c) Mlinaric-Majerski, K.; Visnjevac, A.; Kragol, G.; Kojic-Prodic, B. *J. Mol. Struct.* **2000**, *554*, 279. (d) Dyer, R. B.; Ghirardelli, R. G.; Palmer, R. A.; Holt, E. M. *Inorg. Chem.* **1986**, *25*, 3184.

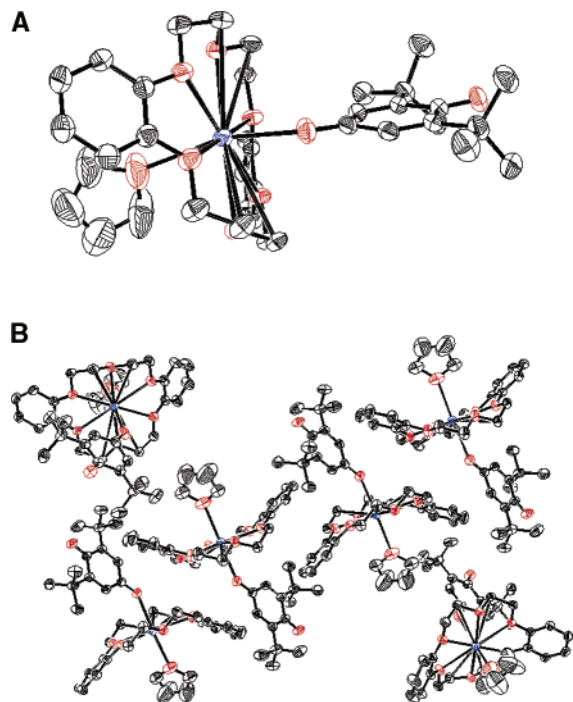


Figure 4. (A) ORTEP diagram and (B) crystal packing of $\text{K}(\text{crown ether})^+\text{m-B}_2\text{Q}^{\bullet-}$, showing the nesting of K^+ in the crown-ether ligand.

anion radical, one potassium cation lying within the cavity of the crown-ether, and three THF solvates (space group: $P2_1/n$). Notably, X-ray analysis reveals that only a single oxygen of the quinone is coordinated to the potassium cation (Figure 4). The other (sterically hindered) carbonyl group of the anion radical remains uncoordinated, and one of the positions in the coordination sphere of the potassium cation is occupied by THF solvate. Thus, instead of the formation of infinite chains, $\text{m-B}_2\text{Q}^{\bullet-}$ and $\text{K}(\text{crown ether})^+$ form a more or less discrete ion pair (Figure 4B). The potassium–oxygen separation of 2.61 Å in this salt has the shortest K–O distance; and the K–O–C and K–O–C–C (dihedral) angles are 142° and 11° , respectively.

II. Quinone Structural Changes upon One-Electron Reduction. A. Molecular Structures in Separated Ion Pairs. The significant interionic separations of $r_{\text{SIP}} > 5$ Å extant in separated ion pairs essentially ensure that the X-ray structures of the anion-radical moiety represent those of the unencumbered ions;²¹ Table 1 lists how the principal (C–C) bond lengths undergo selective changes upon one-electron reduction. Therefore, the basic structural characteristics measured in their salts with either $\text{K}(\text{cryptand})^+$ or $\text{Na}(\text{cryptand})^+$ (column 4 in Table 1) represent those of the essentially free (undisturbed) anion radicals. For comparison, the relevant bond lengths of the corresponding parent quinone (**Q**) and the fully reduced

Table 1. Principal Bond Lengths (in Å)^a Characteristic of the Separated Anion Radical ($\text{Q}^{\bullet-}$), the Neutral Quinone Acceptor (**Q**), and the Corresponding Hydroquinone (H_2Q)

| | bond | Q | $\text{Q}^{\bullet-}$ ^b | H_2Q | q_i ^c | q^f |
|-------------------------|------|--------------------|-------------------------------------|---|------------------------------|-------------------|
| BQ | a | 1.223 ^d | 1.267(2) [1.271(1)] ^e | 1.377 ^f | 0.29 [0.31] ^e | 0.40 ± 0.08 |
| | b | 1.473 ^d | 1.439(2) [1.428(1)] ^e | 1.382 ^f | 0.37 [0.49] ^e | |
| | c | 1.334 ^d | 1.354(2) [1.356(1)] ^e | 1.383 ^f | 0.41 [0.44] ^e | |
| DQ | a | 1.217 ^g | 1.272(3) | 1.393 ^h | 0.31 | 0.41 ± 0.16 |
| | b | 1.478 ^g | 1.449(3) | 1.393 ^h | 0.34 | |
| | c | 1.325 ^g | 1.378(3) | 1.406 ^h | 0.65 | |
| CA | a | 1.211 ⁱ | 1.248(1) | 1.336 ^j | 0.30 | 0.38 ± 0.06 |
| | b | 1.489 ⁱ | 1.448(1) | 1.392 ^j | 0.42 | |
| | c | 1.344 ⁱ | 1.360(1) | 1.388 ^j | 0.36 | |
| p-B₂Q | a | 1.217(2) | 1.269(1) | 1.389 ^k | 0.30 | 0.39 ± 0.10 |
| | b | 1.483(2) | 1.450(1) | 1.391 ^k | 0.36 | |
| | c | 1.335(2) | 1.368(1) | 1.396 ^k | 0.53 | |
| m-B₂Q | a | 1.252 ^l | 1.268(6) [1.462] ^{l,m} | 1.399 ⁿ [1.434(8)] ^m | 0.25 [1.375] ⁿ | 0.38 ± 0.14^o |
| | b | 1.502 | 1.471(9) | 1.401 | 0.37 | |
| | c | 1.345 ^l | 1.372(9) | 1.396 ⁿ | 0.55 | |

^a Average of the corresponding bonds (within 3σ); esd's of mean values given in parentheses are calculated from the experimental esd as $\sigma = (\sum (1/\sigma_i)^2)^{-1/2}$. ^b From $\text{K}(\text{cryptand})^+\text{Q}^{\bullet-}$ salt in all cases except $\text{Na}(\text{cryptand})^+\text{CA}^{\bullet-}$. ^c Contribution of benzenoid structures, see text. ^d Reference 3a. ^e In brackets, polymorph II. ^f Reference 22a. ^g Reference 3b. ^h Reference 22b. ⁱ Reference 22e. ^j Reference 22c. ^k Reference 22d. ^l Bond lengths in 2,6-di-*tert*-butyl-4-methoxyphenol²³ (crystal structure of corresponding H_2Q not available). ^m In brackets, bond lengths of unsubstituted end. ⁿ Reference 3c. ^o Based on 2,6-di-*tert*-butyl-4-methoxyphenol²³ as H_2Q .

hydroquinone (H_2Q) are also presented in Table 1 (columns 3 and 5), so that the structural changes in the quinone moiety can be identified in the most unambiguous way.

The bond lengths within the anion radical of the parent (unsubstituted) benzoquinone are essentially the same in both of its polymorphs, and this confirms the minimal disturbance of the $\text{BQ}^{\bullet-}$ moiety by its counterion. In agreement with the SOMO character (which is antibonding with respect to both double bonds and bonding with respect to carbon–carbon single bonds of *p*-benzoquinone⁸), all the anion radicals show consistent lengthening of the C=O and C=C bonds and some shortening of C–C bonds as compared to those in the parent acceptor (Table 1). Such structural changes place the anion-radical intermediate between the *quinonoid* structure of the quinone **Q** and *benzenoid* structure of the hydroquinone (H_2Q).

To quantify the quinonoid/ benzenoid character of the anion radical, we calculate the average ratio (q) of (i) the bond length difference between the anion radical and the parent acceptor (i.e., $\Delta d_i(\text{Q}^{\bullet-}) = d_i(\text{Q}^{\bullet-}) - d_i(\text{Q})$) relative to (ii) the bond length difference between the same bond in the hydroquinone and quinone (i.e., $\Delta d_i(\text{H}_2\text{Q}) = d_i(\text{H}_2\text{Q}) - d_i(\text{Q})$):²⁴

$$q = 1/n \sum q_i = 1/n \sum \{\Delta d_i(\text{Q}^{\bullet-}) / \Delta d_i(\text{H}_2\text{Q})\} \quad (2)$$

In eq 1, d_i refers to the length of a particular bond (a, b, or c), such that $q_i = \Delta d_i(\text{Q}^{\bullet-}) / \Delta d_i(\text{H}_2\text{Q})$ represents the benzenoid contribution based on the length differences of the single bond.

(21) See discussion of structures of separated anion radicals of (di)nitrobenzene derivatives in ref 17.

(22) (a) Wallwork, S. C.; Powell, H. M. *J. Chem. Soc., Perkin Trans. 2* **1980**, 641. (b) Pennington, W. T.; Patil, A. O.; Curtin, D. Y.; Paul, I. C. *J. Chem. Soc., Perkin Trans. 2* **1986**, 1557. (c) Sikka, S. K.; Chidanbaran, R. *Acta Crystallogr.* **1967**, *23*, 107. (d) Ermer, O.; Robke, C. *Angew. Chem., Int. Ed. Engl.* **1994**, *33*, 1755. (e) van Weperen, K. J.; Visser, G. J. *Acta Crystallogr., Sect. B* **1972**, *28*, 338. Note that the short intermolecular C–O distance of 2.77 Å in crystalline **CA** is much closer than a sum of van der Waals radii of 3.2 Å, and a preliminary study indicates the presence of the (3, -1) critical point indicative of intermolecular “bonding” between these atoms. Davis, W. M. Unpublished results.

(23) Burton, G. W.; Le Page, Y.; Gabe, E. J.; Ingold, K. U. *J. Am. Chem. Soc.* **1980**, *102*, 7791.

(24) (a) Pauling, L. *Nature of the Chemical Bond*; Cornell: Ithaca, NY, 1960. (b) Lindeman, S. V.; Rosokha, S. V.; Sun, D.-L.; Kochi, J. K. *J. Am. Chem. Soc.* **2002**, *124*, 843.

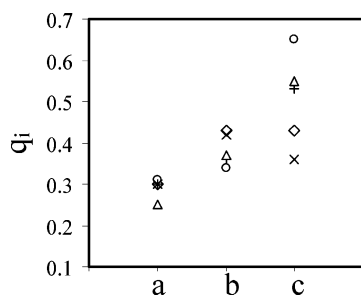


Figure 5. Ratio (q_i) of the difference $\Delta d_i(\text{Q}^{\bullet-})$ between the length of bond $i = a, b,$ or c in the anion radical and the quinone acceptor relative to the difference of the corresponding bond length $\Delta d_i(\text{H}_2\text{Q})$ between the hydroquinone and the quinone: **BQ** (◇); **DQ** (○); **CA** (×); ***p*-B₂Q** (△); ***m*-B₂Q** (+)

Thus, the average value of $q = 1/n \sum\{(\Delta d_i(\text{Q}^{\bullet-})/\Delta d_i(\text{H}_2\text{Q}))\} = 0.40 \pm 0.08$ (where n is the number of bonds) indicates that the anion-radical structure is roughly midway between the quinone and hydroquinone structures, with a benzenoid contribution of about 40% and a quinonoid contribution of approximately 60%.

As seen from the penultimate column in Table 1, the values of q_i for each quinone varies notably depending on the choice of the bond (e.g., for **BQ**^{•-}, q_i fluctuates from 0.29 to 0.49). Such scattering is partly due to the accuracy of measurements of relatively small differences in bond lengths, which are roughly an order of magnitude higher than the estimated standard deviation (esd) σ . However, the comparison of the data for several quinone derivatives in Figure 5 suggests the presence of statistically significant differences in the variation of q_i . Thus, while the calculations based on the lengths of the b and c bonds are in the 0.4–0.6 range, the corresponding values based on the C=O bond (a) are notably less, i.e., 0.29 ± 0.02 . Such a deviation in the relative bond length changes upon reduction may be an intrinsic property of anion radicals, but they may also be related to the choice of hydroquinone as the reference structure (since the presence of hydrogen in the latter may lead to a disproportionate elongation of the C–O bonds).

The reductions of the permethyl-substituted duroquinone (**DQ**), the di-butyl-substituted quinones, ***m*-B₂Q** and ***p*-B₂Q**, to their anion radicals result in bond length changes similar to those found in the parent **BQ**. Thus, the bond length-based estimates of the benzenoid contribution to the anion-radical structure produces an average value of $q = 0.39 \pm 0.10$. Moreover, the data in Table 1 confirm that the geometric characteristics of the corresponding species (prepared as separated ion pair salts with cryptand-ligated counterions) lie mostly within 3σ of that in the parent **BQ**^{•-}. The only significant deviation is observed with the *meta*-di-*tert*-butyl-substituted quinone in which the value of the C–C single bond can vary significantly, i.e., $d_b = 1.471 \text{ \AA}$ in the fragment containing the *tert*-butyl substituents and $d_b = 1.434 \text{ \AA}$ at the opposite end of the quinone. However, in the corresponding neutral acceptor, the b bond length on opposite ends of the ring differ even more noticeably ($d_b = 1.502$ and 1.462 \AA); and we conclude that this discrepancy may be related to steric as well as electronic effects induced by the bulky alkyl groups.

The geometry of the chloranil anion radical (**CA**^{•-}) in separated ion-pair salts also deviates measurably from that of the unsubstituted and alkyl-substituted analogues. As such, **CA**^{•-} is characterized by a much shorter C=O bond (although the

carbon–carbon bonds are similar to those in other anion radicals in Table 1). This distinction is probably related to the withdrawal of electron density by the four electronegative (chlorine) substituents.

It is also to be noted that earlier DFT computations⁸ predict the structural changes in the quinone upon reduction to its anion radical, although even the recently calculated values of $d_a = 1.266 \text{ \AA}$, $d_b = 1.464 \text{ \AA}$, and $d_c = 1.383 \text{ \AA}$ ^{9b} overestimate the double-bond elongation and structurally place the anion radical somewhat closer to the hydroquinone ($q = 0.46$) than that observed experimentally. By way of contrast, the Hartree–Fock approach^{7c} is found to give a larger weight to the quinonoid resonance structure, (e.g., short C=O and C=C bond lengths of $d_a = 1.211 \text{ \AA}$ and $d_c = 1.330 \text{ \AA}$, respectively, and a long C–C bond length of $d_b = 1.483$) as compared to the experimental structure of the quinone anion radicals presented herein.

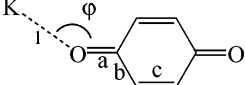
B. Molecular Structures in Contact Ion Pairs. The distinctive effects of contact ion pairing on anion-radical structures are manifested in two structural classes of direct metal-ion coordination, as follows.

1. *Symmetrical binding* involves contact ion pairs in infinite chains in which each K^+ axially coordinates a pair of quinone anion radicals (via their oxygen centers), or viewed alternatively, every anion radical is directly bonded at each of their oxygen termini to an alkali-metal cation. This type of contact ion pairing is observed above in the parent benzoquinone anion-radical salt: $\text{K}(\text{crown ether})^+\text{BQ}^{\bullet-}$ (Figure 2) and in the *p*-di-*tert*-butyl-substituted salt $\text{K}(\text{THF})_4^+\text{p-B}_2\text{Q}^{\bullet-}$ (Figure 3).

Thus in $\text{K}(\text{crown ether})^+\text{BQ}^{\bullet-}$, the potassium cation is bonded to both oxygens of the benzoquinone anion radical with slightly different separations of about 2.7 \AA (Table 2). The most noticeable effect of such direct potassium coordination is the fact that the C–C single bonds (b) are about 0.02 \AA shorter in the contact ion pair (CIP) than that in the corresponding anion radical of the separated ion pair (SIP). In addition, such a coordination leads to inequivalent C=C bonds within the anion radical, while their averaged value is essentially the same as that in separated **BQ**^{•-} species. The carbonyl bonds are unchanged in anion-radical moieties from both CIP and SIP salts. Although the shorter C–C single bonds (b) within the symmetrically ion-paired **BQ**^{•-} anion radical places it somewhat closer to the benzenoid structure than the separated one, the estimated average value of $q = 0.45$ characteristic of the anion radical in CIP (Table 2) is still within the accuracy limit of that of the SIP structures in Table 1.

In the salt $\text{K}(\text{THF})_4^+\text{p-B}_2\text{Q}^{\bullet-}$, the mode of ion pairing with a symmetrical K–O separation of 2.607 \AA is quite similar to that in the $\text{K}(\text{crown ether})^+\text{BQ}^{\bullet-}$ salt. The geometry of the ion-paired ***p*-B₂Q**^{•-} moiety is even closer to that of the corresponding separated anion radical, with all the corresponding bond lengths characteristic of the CIP and SIP structures being within 3σ . As such, we conclude that a pair of symmetrically bonded counterions do not perceptibly disturb the geometry of the quinone anion radical.

2. *Unsymmetrical binding* occurs in the second type of ion pairing observed in the anion-radical salts of $\text{K}(\text{crown ether})^+\text{m-B}_2\text{Q}^{\bullet-}$ which shows isolated 1:1 complexes in which only one quinone anion radical is coordinated to the potassium counterion and the opposite axial position of the cation is occupied by THF solvates (Figure 4). Since the sterically hindered carbonyl group

Table 2. Principal Bond Lengths (in Å)^a and Angles (in Deg) Characteristic of the Quinone Structures in Contact Ion Pairs


| salt | <i>l</i> | φ^a | θ^b | <i>d</i> _a | <i>d</i> _b | <i>d</i> _c | <i>q</i> ^c |
|--|-----------------------|-------------|------------|-----------------------|-----------------------|-----------------------|-----------------------|
| K(crown ether) ⁺ BQ ^{-•} | 2.647(4) | 117 | 112.6 | 1.268(5) | 1.421(6) | 1.337(6) | 0.45 |
| | 2.734(4) ^d | 111 | 119 | 1.270(5) | 1.417(6) | 1.368(6) | |
| K(THF) ₄ ⁺ p-B₂Q ^{-•} | 2.623(2) | 149.9 | 136 | 1.268(3) | 1.429(6) | 1.357(3) | 0.42 |
| | | | | | 1.426(6) | | |
| K(crown ether) ⁺ m-B₂Q ^{-•} | 2.608 | 142.2 | 11.1 | 1.283(3) ^e | 1.430(3) ^e | 1.371(4) | 0.30 ^e |
| | | | | 1.268(3) ^f | 1.432(4) ^e | | 0.28 ^f |
| | | | | | 1.477(4) ^f | | |
| | | | | | 1.466(4) ^f | | |

^a K–O–C angle. ^b K–O–C–C dihedral angle. ^c Contribution of the benzenoid form; see Table 1. ^d Distances and angles characteristic of the coordination of the potassium to the opposite ends of the quinone are slightly different. ^e Coordinated end. ^f Noncoordinated end.

Table 3. Hyperfine Splitting Constants^a of Separated and Contact Ion Pairs of Quinone Anion Radical, and Their (1:1) Associates with Neutral Quinone

| Q | K(cryptand) ⁺ Q ^{-•} | K(crown ether) ⁺ Q ^{-•} | K(THF) _n ⁺ Q ^{-•} | K(cryptand) ⁺ Q ^{-•} ·Q |
|-------------------------|--|---|---|---|
| BQ | 2.42 (4H) | 1.91 (2H _β), 2.93 (2H _α) ^b | 1.77 (2H _β), 3.03 (2H _α) ^c | 1.50 (2H _β), 3.32 (2H _α) |
| p-B₂Q | 2.34 (2H) | 1.85 (1H _β), 2.65(1H _α) ^g | 1.77 (1H _β), 2.81 (1H _α) | 1.56 (1H _β), 3.12 (1H _α) ^e |
| m-B₂Q | 2.30 (2H) | 1.75 (2H _β) | 1.79 (2H _β) ^d | 1.60 (2H _β) |
| DQ | 1.90 (12H) ^e | | 1.43 (6H _β), 2.41 (6H _α) ^f | 1.27 (6H _β), 2.54 (6H _α) ^e |

^a In units of G; in parenthesis, number of splitting hydrogen. ^b Fast counterion jumps at room temperature led to averaged value: *a* = 2.42 G (4H). ^c In EtCN; fast counterion jumps at room temperature led to the averaged value: *a* = 2.43 (4H). ^d *a* = 1.62 (2H) at –80. ^e Reference 26. ^f In DME, ref 6a. ^g In DME, ref 6d.

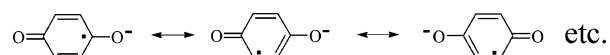
remains uncoordinated, the K–O bonding at 2.61 Å with one carbonyl group in the K(crown ether)⁺**m-B₂Q**^{-•} provides the unsymmetrical disturbance of the anion radical. For example, the carbon–oxygen bond length at the “contact” end is 1.283 Å as compared to the value of 1.268 Å characteristic of the corresponding “noncontact” bond. The average carbon–carbon bond length adjacent to the “contact” end is 1.431 Å, while at the “noncontact” end the corresponding value is 1.472 Å. Thus, the bond length changes relative to the neutral acceptor are more pronounced at the coordinated end. Accordingly, the calculated benzenoid contribution based on the *a* and *b* bond lengths measured on the “coordinated” half of benzoquinone is 0.30, while that based on the bond length of the noncoordinated half is 0.28. [Note, that the calculations of *q* are based on the relative bond length changes in the 2,6-di-*tert*-butyl-substituted quinone (**m-B₂Q**), the anion-radical (**m-B₂Q**^{-•}), and the hydroquinone **H₂(m-B₂Q)** moieties and, thus, are not affected by the differences resulting from the unsymmetrical location of *tert*-butyl groups.] It thus corresponds to the unsymmetrical distribution of the additional unpaired electron, with the electron density being slightly shifted closer to the potassium-coordinated end.

III. Interrelationship between X-ray Structures of Quinone Anion Radicals in the Solid State vs Their Dynamic Behavior in Solution as Separated and Contact Ion Pairs. Although X-ray crystallographic analysis constitutes the most suitable technique for definitive measurements of bond length effects in the solid state, it requires a complementary experimental methodology for probing dynamic structures in solution. Since the latter has been provided by electron paramagnetic resonance (EPR) spectroscopy for quinone anion radicals (Q^{-•}) of interest in this study,^{6,12–14} our task now is to comment on the X-ray structures of separated and contact ion pairs in Tables 1 and 2, respectively, relative to their solution EPR characteristics in four (separate) ways.

A. EPR Spectra and the Odd-Electron (Spin) Distribution in SIP Structures. The dissolution of the separated ion-pair salt: K(cryptand)⁺**BQ**^{-•} in THF affords an EPR spectrum characterized by well-resolved hyperfine splittings from four equivalent hydrogens with a hyperfine splitting constant of *a*_{4H} = 2.42 G (Table 3, and Figure S8 in the Supporting Information). This spectrum is essentially temperature-independent with only a slight line narrowing upon lowering the temperature from 313 to 193 K. The binominal quintet splitting corresponds to symmetrical delocalization of the electron density over the entire quinone framework.²⁵ Similarly, THF solutions of the di-*tert*-butyl (alkyl) substituted anion-radical salts K(cryptand)⁺**m-B₂Q**^{-•} and K(cryptand)⁺**p-B₂Q**^{-•} are characterized by temperature-independent EPR spectra showing hyperfine splitting by two equivalent ring hydrogens, and a duroquinone anion radical (**DQ**^{-•}) shows twelve equivalent hydrogens from four methyl groups. The values of the proton hyperfine splittings of both **m-B₂Q**^{-•} and **p-B₂Q**^{-•} are rather close to that of parent **BQ**^{-•} (Table 3) indicating only a relatively minor modulation of the electron distribution by the sterically hindering *tert*-butyl groups. It is also important to note that the hyperfine splittings observed in solutions of quinone anion radicals with cryptand-encapsulated potassium counterions are essentially the same as those reported earlier for the corresponding “free” anion radicals.^{13,14}

B. Spin Distribution and Counterion Migration in Contact Ion Pairs. In strong contrast to separated ion pairs, the

(25) (a) Such a spin distribution in terms of valence-bond description represents the contribution of all the classical resonance structures:



(b) Note that the EPR spectra of the yellow to brown crystalline SIP/CIP salts of quinone anion radicals consisted of broad envelopes which we were unable to resolve into their hyperfine components.
(26) Suga, K.; Takiguchi, T.; Aoyagui, S. *Bull. Chem. Soc. Jpn.* **1986**, *59*, 1433.

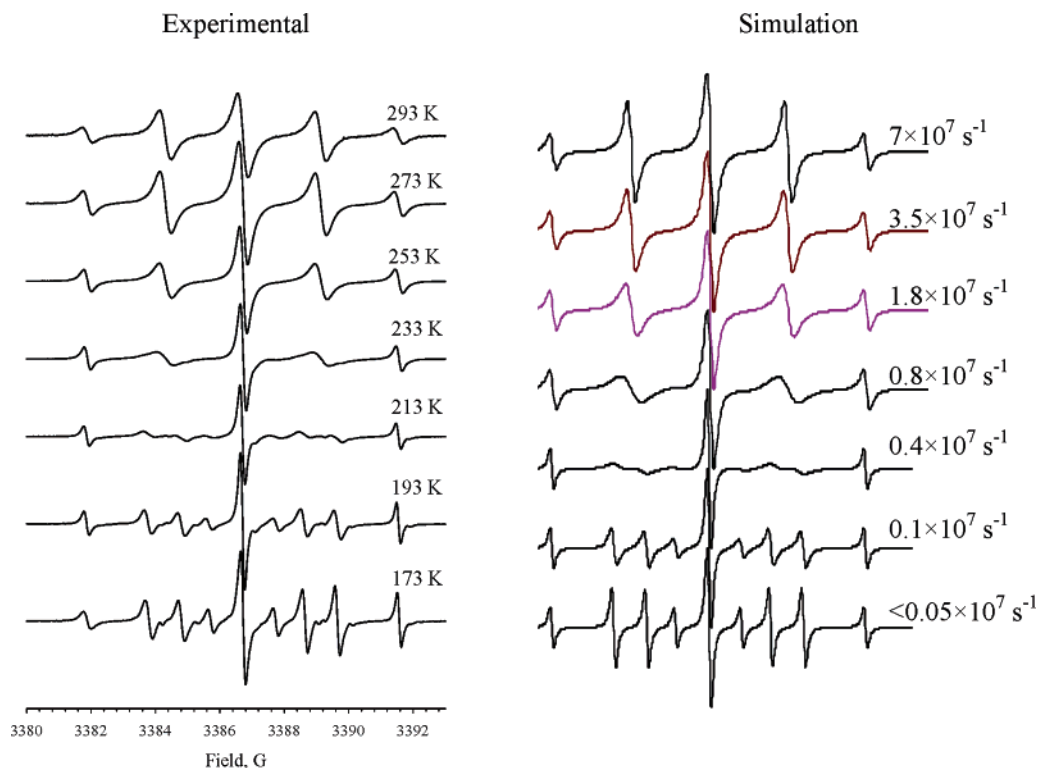
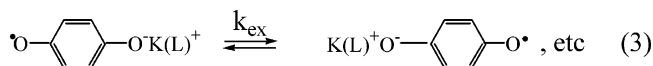


Figure 6. Temperature-dependent EPR spectra of $\text{K}(\text{crown ether})^+\text{BQ}^{\bullet-}$ in THF (left) and their dynamic EPR simulation (right) based on exchange of two sets of two nonequivalent hydrogens (with $a = 2.93$ and 1.91 G for each pair) and first-order rate constant for exchange (k_{ex}) as indicated.

dissolutions into THF of the quinone anion-radical salts with crown-ether coordinated potassium counterions afford EPR spectra which show a significant dependence on the temperature. For example, the EPR spectrum of the THF solution of $\text{K}(\text{crown ether})^+\text{BQ}^{\bullet-}$ at room temperature is similar to that of $\text{K}(\text{cryptand})^+\text{BQ}^{\bullet-}$, both spectra showing the binominal quintet derived from splittings on four equivalent hydrogens with a hyperfine constant of $a = 2.42$ G. However, lowering the temperature of the $\text{K}(\text{crown ether})^+\text{BQ}^{\bullet-}$ solution results in the selective broadening and subsequent disappearance of the hyperfine components with $M = \pm 1$, and at very low temperature the EPR spectrum shows the splittings of the two inequivalent pairs of hydrogens (Figure 6) with $a_{\text{H}\alpha} = 2.93$ and $a_{\text{H}\beta} = 1.91$ G. Such alternating line broadenings and spectral transformations were observed earlier in the solution of quinone anion radicals with alkali-metal counterions (in the presence of crown-ether or without any additional ligands) and were assigned to reversible switching of the counterion coordination from one end of benzoquinone to the other.^{6,12,13} Thus, the covalent coordination of the quinone anion radical to the alkali-metal counterion at one end is accompanied by a significant shift of the electron spin, and two pairs of protons become significantly inequivalent.²⁷ Such a migration of the counterion from one end to the other that leads to alternating line broadenings can be effectively described as either a “counterion

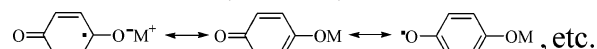
jump” or “benzoquinone turnaround” for the overall CIP transformation in eq 3.



At low temperatures, the rate of this process is slow on the EPR time scale, and dynamic EPR simulation produces the value of the rate constant: $k_{\text{ex}} \approx 1 \times 10^6 \text{ s}^{-1}$ at -80 °C. As such, the “frozen” spectrum reveals an unsymmetrical electron distribution with a significant difference in the proton hyperfine splitting constants at the “coordinated” and “uncoordinated” ends. As the temperature increases, the rates of the switching become faster, such that at room temperature it is very fast on the EPR time scale, and the spectra reveal “averaged” splittings by four equivalent hydrogens.²⁸ Dynamic EPR simulation leads to a rate constant of $k_{\text{ex}} \approx 7 \times 10^7 \text{ s}^{-1}$ at 20 °C. Essentially the same EPR behavior is observed for the benzoquinone anion radical produced in situ by potassium-mirror reduction in THF solutions without the addition of any extra ligand (L), the only difference being a somewhat larger difference of the splitting of the inequivalent pairs of hydrogens in Table 1.

EPR spectroscopy of THF solutions of either $\text{K}(\text{crown ether})^+p\text{-B}_2\text{Q}^{\bullet-}$ or $\text{K}(\text{THF})_4^+p\text{-B}_2\text{Q}^{\bullet-}$ also show alternating line broadening (Figure 7).^{12,13} At low temperatures, the exchange is relatively slow ($k_{\text{ex}} < 10^6 \text{ s}^{-1}$ at $T < -60$ °C), and the EPR spectrum shows a doublet of doublets derived from the splittings on two inequivalent hydrogens (Table 3). At room temperature,

(27) (a) Such a “frozen structure” represents the contact ion pair in which spin redistribution results from (valence-bond) resonance forms:



(b) Spin distribution in this contact ion pair is directly related to that calculated for the protonated quinone anion radical ($\text{HQ}^{\bullet-}$).^{8d}

(28) The (room-temperature) ESR spectrum resulting from the fast exchange is the same as that from the (temperature-independent) separated ion pair, but in this case it represents the “averaged” spectrum arising from the dynamic process (eq 3) and its temperature dependence is modulated via k_{ex} .

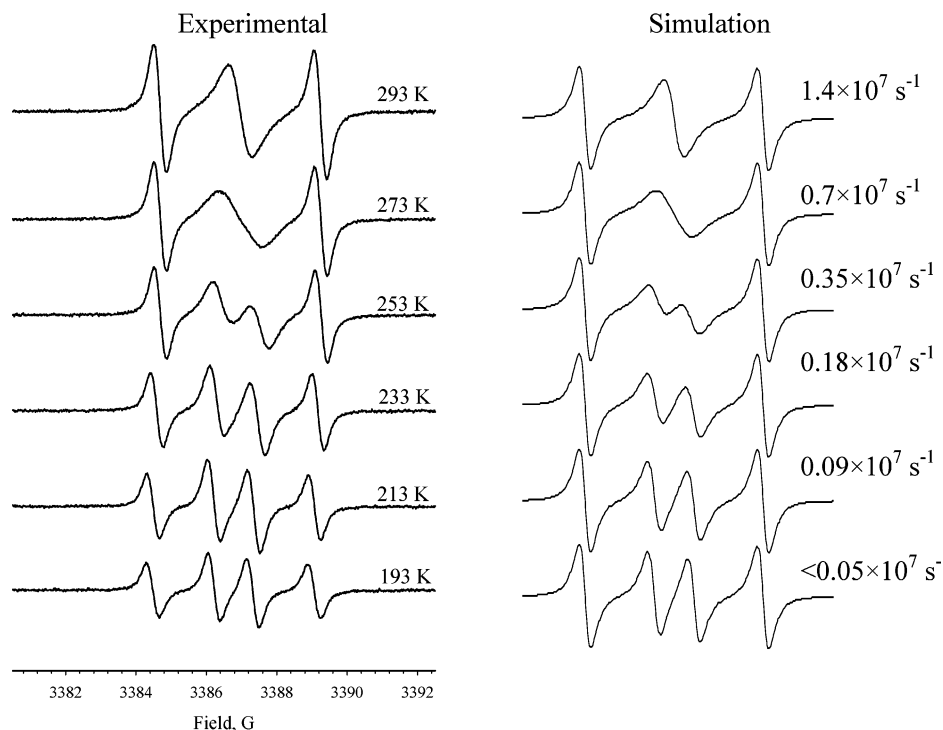
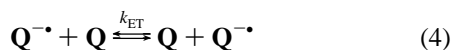


Figure 7. Temperature-dependent EPR spectra of $\text{K}(\text{THF})_4^+p\text{-B}_2\text{Q}^{\bullet-}$ in THF (left) and their dynamic ESR simulation (right) based on exchange of two sets of two nonequivalent hydrogens (with $a = 2.93$ and 1.91 G for each pair) with the first-order rate constants of exchange (k_{ex}) as indicated.

the rate of counterion jump is fast on the EPR time scale ($k_{\text{ex}} = 1.4 \times 10^7 \text{ s}^{-1}$) and produces the binominal triplet corresponding to the averaged splitting on two hydrogens.

A pair of *tert*-butyl groups in the ortho position hinders the coordination of potassium counterion to one end and prevents the counterion jumps in $m\text{-B}_2\text{Q}^{\bullet-}$ anion radical. As a result, the EPR spectrum of the solutions of $m\text{-B}_2\text{Q}^{\bullet-}$ with $\text{K}(\text{crown ether})^+$ or $\text{K}(\text{THF})_n^+$ counterions show the same triplet as the spectrum of the separated anion radical derived from $\text{K}(\text{cryptand})^+m\text{-B}_2\text{Q}^{\bullet-}$ salt (i.e., $k_{\text{ex}} = 0$). However, the ion-paired anion radicals are characterized by considerably lower values of the splitting constant (compare columns 3/4 with column 2 in Table 3), and this indicates that the carbonyl group at the open end of $m\text{-B}_2\text{Q}^{\bullet-}$ is largely coordinated to the potassium cation. This leads to the same shift of the spin density to one end of 2,6-di-*tert*-butyl-substituted benzoquinone, in accord with X-ray structural data (vide supra).

C. EPR Spectra Accompanying Electron-Transfer Self-Exchange of Quinone Anion Radicals with Their Parent Acceptors. The general line broadening of the well-resolved hyperfine splittings of the quinone anion radical (**Q** in Table 2) observed upon incremental additions of quinone acceptors in solution is known from the seminal studies of Adams, Fessenden and co-workers¹⁴ to arise from the bimolecular electron-transfer self-exchange between the paramagnetic anion radical and its diamagnetic parent, i.e.,



Thus, the second-order rate constants of $k_{\text{ET}} = 8.1 \times 10^7$ and $1.24 \times 10^8 \text{ M}^{-1} \text{ s}^{-1}$ were measured for *p*-benzoquinone and duroquinone anion radicals generated in situ with the encumbered Bu_4N^+ counterion.¹⁵ Similar rate constants of k_{ET}

$= 6.2 \times 10^7$ and $2.0 \times 10^8 \text{ M}^{-1} \text{ s}^{-1}$ were also measured for **BQ**^{•-} and **DQ**^{•-} in aqueous solution,^{14b} and the rate constants in the polar aprotic solvent dimethylformamide (DMF) are $k_{\text{ET}} = 3.8 \times 10^8$ and $6.2 \times 10^7 \text{ M}^{-1} \text{ s}^{-1}$.^{14a} The rather uniform rate constants measured under these conditions suggest that these (in situ) generated quinone anion radicals exist as separated ion pairs in such environments. This separated ion-pair nature is indeed confirmed by our measurements of essentially the same second-order rate constant of $k_{\text{ET}} \approx 2 \times 10^8 \text{ M}^{-1} \text{ s}^{-1}$ when the crystalline separated ion pair (SIP) salt $\text{K}(\text{cryptand})^+\text{BQ}^{\bullet-}$ is directly dissolved in THF solutions containing various (small) amounts of **Q**, and then measuring the accompanying changes in the EPR line widths at decreasing temperatures. However, close inspection of the temperature-dependent EPR spectrum reveals the admixture of a new paramagnetic component, species “X”, which is especially prevalent at low temperatures as illustrated in Figure 8. The hyperfine splitting patterns of species “X” are described in Table 3 (last column) for some of the quinones in Chart 1, and their structural identification is described in the next section. Moreover, the complex temperature-dependent line broadening behavior observed with the contact ion pair $\text{K}(\text{crown ether})^+\text{BQ}^{\bullet-}$ dissolved in THF together with **BQ** is somewhat comparable to those observed with the SIPs, but the difference is insufficient to precisely dissect out the contribution from the facile counterion migration described in eq 3.²⁹

(29) (a) For comparative purposes, the EPR line broadenings in solutions of $\text{K}(\text{crown ether})^+\text{BQ}^{\bullet-}$ in the presence of various amounts of **BQ** yield the approximate rate constant: $k_{\text{ET}} \approx 0.4 \times 10^8 \text{ M}^{-1} \text{ s}^{-1}$ (at 20 °C). (b) The chain character of the contact ion pair, as established by X-ray crystallography in Figure 2, raises the question as to the role that such multibonded “oligomers” may play in dynamic processes in solution. As such, their presence must be explicitly taken into account in the quantitative evaluation of the phenomenological rate constants obtained by EPR line broadening studies.

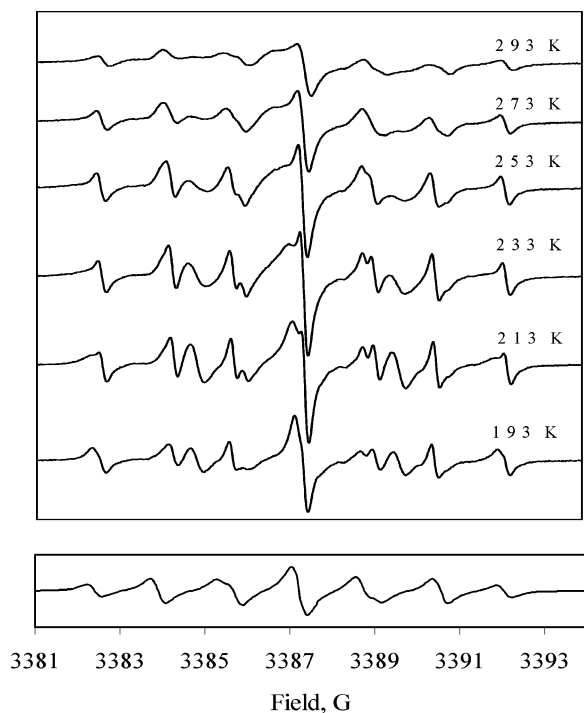


Figure 8. (Upper) A series of temperature-dependent EPR spectra of $\text{K}(\text{cryptand})^+\text{BQ}^{\bullet-}$ in the presence of BQ in THF showing an additional component (species “X”) with its relative intensity increasing at lower temperatures. (Lower) Computer simulation with $a_{2\text{H}\alpha} = 3.32$ and $a_{2\text{H}\beta} = 1.50$ G in Table 3.

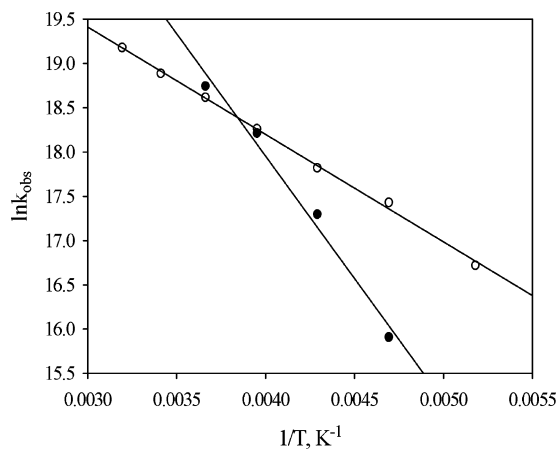


Figure 9. Arrhenius plot for the self-exchange electron transfer between the $p\text{-B}_2\text{Q}^{\bullet-}$ anion radical and the corresponding neutral acceptor in THF with a potassium counterion in the presence of cryptand (○) or without cryptand (●).

Accordingly, we turn to the symmetrical and unsymmetrical di-*tert*-butyl-substituted quinones, $p\text{-B}_2\text{Q}^{\bullet-}$ and $m\text{-B}_2\text{Q}^{\bullet-}$, respectively, in our attempt to compare SIP and CIP reactivities.

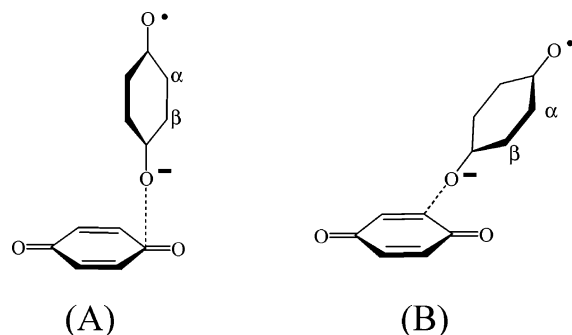
Our kinetic measurements based on the EPR line broadenings of the symmetrically di-*tert*-butyl-substituted quinone anion radical salt $\text{K}(\text{cryptand})^+p\text{-B}_2\text{Q}^{\bullet-}$ dissolved in THF afford the second-order rate constant $k_{\text{ET}} = 1.6 \times 10^8 \text{ M}^{-1} \text{ s}^{-1}$ at 293 K to represent separated ion-pair reactivity. The temperature dependence of the second-order rate constants ($\ln k_{\text{ET}}$) with inverse temperature in Figure 9 shows linear character and yields an overall activation barrier of $\Delta H_{\text{ET}} = 2.4 \text{ kcal mol}^{-1}$ for $p\text{-B}_2\text{Q}^{\bullet-}$ as expected from the $\text{K}(\text{cryptand})^+$ salt of the SIP. Likewise, the comparative self-exchange behavior of the cor-

responding CIP salt is studied under the same conditions but without the presence of [2,2,2]cryptand. The temperature dependence of the self-exchange rate constant (k_{ET}) shows a larger slope (Figure 9) which indicates that the apparent activation barrier for self-exchange is substantially higher ($\Delta H_{\text{ET}} \approx 5.7 \text{ kcal mol}^{-1}$) than that of the SIP counterpart. A closer inspection of the Arrhenius plot, however, reveals a slight curvature indicative of some multistep process which we tentatively ascribe to the incursion of ion-pair dissociation that is superimposed onto the electron-transfer kinetics of the contact ion pair (vide infra). Thus the EPR line broadening behavior of $p\text{-B}_2\text{Q}^{\bullet-}$ dissolved in THF points to the importance of ion-pair dissociation in the quantitative (kinetics) evaluations of CIP behavior which we hope to address further in a separate study.³⁰

D. EPR Spectra and the Intermolecular Collapse of Quinone Anion Radicals with Their Acceptors in Separated and Contact Ion Pairs. Scrutiny of the temperature-dependent (EPR) spectral changes of the separated ion pair $\text{K}(\text{cryptand})^+\text{BQ}^{\bullet-}$ in THF solutions containing the parent acceptor (BQ in Figure 8) reveals the presence of a minor spectral feature of species “X” (vide supra) in addition to the principal spectrum of the SIP, the relative concentrations of which increase at low temperatures. Indeed, this new spectral component is the same as that reported earlier by Suga,²⁶ and it is thus desirable to emphasize three distinct behavioral characteristics of species “X”. First, the EPR spectrum of “X” is observed only when the quinone and anion radical is prepared as the separated ion-pair salt, the corresponding CIP salt showing no such signs. The latter suggests that direct metal-ion coordination of $\text{Q}^{\bullet-}$ (as in the CIP) hinders the subsequent association with another acceptor owing to the significant neutralization of negative charge. Second, the formation of “X” appears to be quasi-reversible with temperature variation, the new steady-state concentration being relatively quickly attained with $\text{BQ}^{\bullet-}$, $\text{DQ}^{\bullet-}$, and $p\text{-B}_2\text{Q}^{\bullet-}$ but decidedly less so with $m\text{-B}_2\text{Q}^{\bullet-}$ (see Figure S9). Finally but most important, the EPR spectrum in Table 3 (column 5) consists of pairs of proton hyperfine splittings for benzoquinone (BQ), duroquinone (DQ), and *p*-di-butyl-benzoquinone ($p\text{-B}_2\text{Q}^{\bullet-}$) that are similar but yet quite distinct from those of either the separated or the contact ion pair. Thus, the comparison of hyperfine splittings $a_{\text{H}\alpha}$ and $a_{\text{H}\beta}$ in Table 3, column 2 (SIP) and columns 3/4 (CIP) with those in column 5 (species “X”) shows that the ratios $a_{\text{H}\alpha}/a_{\text{H}\beta}$ are larger for “X” than those extant in either the SIP or CIP. Since such a trend is reminiscent of those previously observed in phenoxyl radicals,^{31a} we follow Suga’s proposal that species “X” is an intermolecular $\text{Q}/\text{Q}^{\bullet-}$ complex in which the quinone anion radical is sequestered by its quinone parent (much like they are

(30) (a) See the earlier study of dinitrobenzene anion radicals¹⁸ for the role of ion-pair dissociation in the quantitative determination of electron-transfer kinetics. (b) Self-exchange processes of many planar organic anion radicals were shown earlier^{4a,30b} to proceed via the intermediate π -complex. Moreover, such precursor π -complexes between radicals and their parent diamagnetic molecules have been isolated and characterized for a number of species, including tetrachloro-*p*-benzoquinone (CA) and dichlorodicyano-*p*-benzoquinone (DDQ).^{4a} However, all our efforts to observe the most characteristic feature of such π -complexes, viz, the broad NIR absorption band, with unsubstituted or alkyl-substituted benzoquinone anion radicals have as yet been unsuccessful, even at low temperatures (-90 °C) and highest attainable concentrations of the components. Although the species in Chart 3 appears to have the earmarks of such a precursor complex, its temperature-dependent behavior is not characteristic of such a species (see text). (b) Rosokha, S. V.; Newton, M. D.; Head-Gordon, M.; Kochi, J. K. *Chem. Phys.* **2006**, *324*, 117.

Chart 3



complexed with metal ions in contact ion pairs). Chart 3 illustrates a pair of such proposed “X” structures in which the negative oxygen end of the $Q^{\bullet-}$ dipole is directed either to the electrophilic carbonyl center (A) or to the ring ($C=C$) center (B) of the parent quinone.^{31b,c}

To clarify the structural ambiguity of this complex, we carried out the potassium-mirror reduction of the benzoquinone acceptor in the presence of a cryptand ligand and a large excess of benzoquinone and then allowed the mixture to stand for prolonged periods. The subsequent removal of THF in vacuo followed by crystallization of the residue afforded colorless (diamagnetic) crystals. X-ray analysis of the single crystals established the presence of a pair of 1:1 quinone adducts that are hydrogen-bonded via one proton, and the structural unit thus contains four benzoquinone moieties bearing a unit negative charge that is compensated by $K(\text{cryptand})^+$, the ORTEP diagram of which is presented in Figure 10 (see also Figure S10).

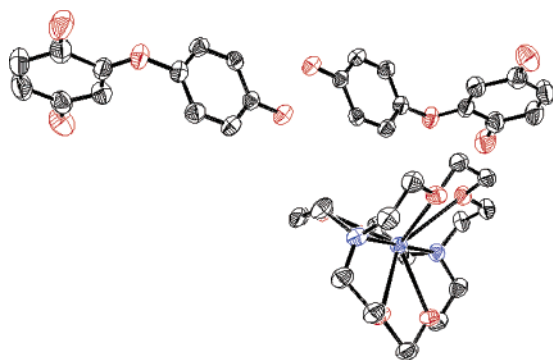
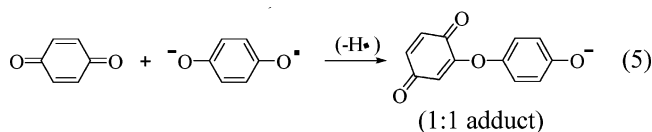


Figure 10. ORTEP diagram of a pair of hydrogen-bonded (1:1) adducts formed in eq 4 upon the collapse of a benzoquinone anion radical and neutral acceptor with a $K(\text{cryptand})^+$ counterion.

(31) (a) Lucarini, M.; Mugnaini, V.; Pedulli, G. F.; Guerra, M. *J. Am. Chem. Soc.* **2003**, *125*, 8318. (b) Phenoxyl radicals generally exhibit splittings of the *ortho*-protons of $a_\alpha = 5.78$ G and the *meta*-protons of $a_\beta = 0.93$ G with $a_\alpha/a_\beta \approx 6$.^{31a} The partial localization of negative charge by metal coordination is accompanied by a spin-density shift to a lower ratio of $a_\alpha/a_\beta \approx 1.5$ in the quinone anion-radical moieties in CIPs.²⁷ Thus, the ratio $a_\alpha/a_\beta \approx 2$ characteristic of the species “X” in Table 3 indicates that the complexation of the anion radical to the parent acceptor (Chart 3) is slightly more intimate and results in a more pronounced charge/spin localization than that by metal-centered counterions examined here. (c) The overall “perpendicular” arrangement in Chart 3A is similar to that found for **CA** in the crystalline state;^{22c} and an analogous structure pertains to the (**DDQ**/**DDQ** $^{\bullet-}$) dyad in Figure S11. Although alternative face-to-face (slipped) orientations of the quinone pair would be related to those already found in precursor complexes for electron transfer,^{4a} they are disfavored for species “X” because its EPR spectrum shows the odd electron to be localized on a single quinone (with significantly inequivalent pairs of splitting protons), whereas it is extensively delocalized between cofacial quinone pairs in precursor complexes.

The structure of the benzoquinone adduct in Figure 10 is thus directly related to structure B in Chart 3 via an *overall* hydrogen-atom loss, i.e.^{31c}



E. Electronic (UV–vis) Spectra of Separated and Contact Ion Pairs.

To further examine some of the deep-seated changes in quinone anion radicals as indicated by their molecular (X-ray) structures and the EPR spectra that accompany the formation of separated versus contact ion pairs, we also examine the corresponding effects on their electronic transitions. In each case, we dissolve the pure crystalline salt for UV–vis measurements to establish their structural identity in THF solutions. The yellow to brown solutions obtained with the separated anion-radical salts of benzoquinone (**BQ**) and duroquinone (**DQ**) with $K(\text{cryptand})^+$ counterion are found to be the same as those of the **CIP** salts with $K(\text{crown ether})^+$ and show only one group of diagnostic absorption bands at $\lambda_{\text{max}} = 420$ and 450 nm in good agreement with the literature data.³² In this regard, our inability to spectrally distinguish the SIP/CIP pairs differs from our earlier observation of such ion pairs of the dinitrobenzene anion radical.^{17,18} The sole exception to the ion-pair effects on the electronic spectra of quinone anion radicals is observed with the unsymmetrical di-*tert*-butyl-substituted derivative $m\text{-B}_2Q^{\bullet-}$ in which the vibronic envelope in the 360–490 window (see Figure S7) differs in the manner somewhat reminiscent of that observed with the dinitrobenzene anion radical.¹⁷ Based on the SIP/CIP equilibrium identified in the latter case, this observation can be tentatively interpreted as the transformation of the contact ion pair at $\lambda_{\text{max}} = 420$ nm into the separated ion pair at $\lambda_{\text{max}} = 450$ nm. This distinction is also analogous to the slow behavior of $m\text{-B}_2Q^{\bullet-}$ in the formation of the intermolecular (X) adduct in Figure S9.

Summary and Conclusions

Direct reduction of various quinones **Q** (Chart 1) with a potassium mirror in the presence of polyether ligands **L** (Chart 2) affords a series of crystalline 1:1 salts, $K(L)^+Q^{\bullet-}$, and X-ray analyses show that the use of $L = [2,2,2]\text{cryptand}$ leads to “separated” ion-pair (SIP) salts, whereas the use of $L = \text{dibenzo-18-crown-6}$ leads to “contact” ion-pair (CIP) salts. The structural changes attendant upon one-electron reduction to anion radicals are then quantitatively evaluated in both SIP and CIP interionic associates in terms of q , the quinonoid/benzenoid bond length parameter in Tables 1 and 2, respectively.

The SIP/CIP dichotomy in the solid state as revealed by such X-ray crystallographic analyses also extends to their solution behavior as revealed by EPR spectroscopy of these crystalline salts dissolved in aprotic (organic) solvents in three distinctive ways. First, the temperature-dependent EPR spectra of CIP salts show selective line broadening symptomatic of a dynamic *site exchange* of $K(L)^+$ between both oxygen centers of $Q^{\bullet-}$ that is diagnostic of such intimately bound ion pairs in eq 3. By contrast, the EPR spectra of SIP salts are temperature indepen-

(32) (a) Kim, Y.-O.; Jung, Y. M.; Kim, S. B.; Park, S.-M. *Anal. Chem.* **2004**, *76*, 5236. (b) Nelsen, S. F.; Weaver, M. N.; Telo, J. P.; Lucht, B. L.; Barlow, S. *J. Org. Chem.* **2005**, *70*, 9326.

Table 4. Crystallographic Parameters and the Details of the Structure Refinements

| compd | K(cryptand) ⁺ BQ ^{•-} (I) | K(cryptand) ⁺ BQ ^{•-} (II) | K(cryptand) ⁺ DQ ^{•-} | K(cryptand) ⁺ p-B ₂ Q ^{•-} | K(cryptand) ⁺ m-B ₂ Q ^{•-} | Na(cryptand) ⁺ CA ^{•-} | K(crown ether) ⁺ BQ ^{•-} | K(THF) ₄ ⁺ p-B ₂ Q ^{•-} | K(crown ether) ⁺ m-B ₂ Q ^{•-} | p-B ₂ Q |
|----------------------|--|---|--|--|--|---|--|--|--|--------------------|
| M | 523.68 | 523.68 | 630.26 | 635.89 | 816.15 | 730.26 | 507.58 | 547.83 | 836.1 | 220.30 |
| space group | P1 | P2(1)/n | P1 | P2 | P2(1)/n | P2(1)/n | P3(1) | P1 | P2(1)/n | P2(1)/n |
| a, Å | 9.178(18) | 10.3668(15) | 11.631(8) | 9.454(4) | 10.143(10) | 15.960(2) | 15.283(3) | 7.992(7) | 16.238(3) | 6.720(7) |
| b, Å | 11.08(3) | 17.507(2) | 11.923(7) | 10.051(4) | 31.03(2) | 12.3063(19) | 15.283(3) | 10.000(10) | 17.760(4) | 10.028(10) |
| c, Å | 13.54(3) | 15.333(2) | 13.901(11) | 20.335(7) | 15.257(13) | 17.062(2) | 9.112(3) | 11.384(11) | 17.190(3) | 9.961(9) |
| α, deg | 91.18(14) | 90 | 93.62(7) | 80.13(4) | 90 | 90 | 90 | 67.94(2) | 90 | 90 |
| β, deg | 99.91(17) | 104.649(13) | 100.27(9) | 84.59(3) | 97.60(9) | 90.431(4) | 90 | 83.77(3) | 109.204(14) | 92.65(8) |
| γ, deg | 92.50(18) | 90 | 103.00(7) | 67.58(3) | 90 | 90 | 120 | 68.12(2) | 90 | 90 |
| V, Å ³ | 1355(5) | 2692.3(8) | 1838(2) | 1759.0(13) | 4759(7) | 3550.9(8) | 1843.3(8) | 781.9(13) | 4681.5(16) | 670.5(11) |
| Z | 2 | 4 | 2 | 2 | 4 | 4 | 3 | 1 | 4 | 2 |
| μ, mm ⁻¹ | 0.244 | 0.245 | 0.192 | 0.199 | 0.165 | 0.572 | 0.265 | 0.208 | 0.169 | 0.071 |
| ρ, g/cm ³ | 1.285 | 1.292 | 1.139 | 1.201 | 1.139 | 1.448 | 1.372 | 1.163 | 1.186 | 1.091 |
| refls | 20 203 | 41 355 | 26 240 | 26 660 | 71 060 | 50 409 | 12 792 | 9142 | 71 198 | 10 038 |
| indpndt | 7756 | 8321 | 9698 | 10 097 | 13 839 | 10 103 | 4079 | 4630 | 14 350 | 2063 |
| obsd | 4818 | 4488 | 4197 | 7461 | 5664 | 5405 | 1705 | 1351 | 7025 | 1615 |
| (F > 2) | | | | | | | | | | |
| R ₁ | 0.046 | 0.046 | 0.059 | 0.039 | 0.084 | 0.044 | 0.039 | 0.055 | 0.065 | 0.0623 |
| (F > 2σ) | | | | | | | | | | |
| wR ₂ | 0.095 | 0.088 | 0.175 | 0.097 | 0.201 | 0.084 | 0.077 | 0.108 | 0.195 | 0.1643 |

dent, as expected for “free” Q^{•-} that is untethered by its counterion. An analogous SIP/CIP distinction is further noted in the rates of *electron-transfer self-exchange* of Q/Q^{•-} dyads in eq 4, although the quantitative comparison awaits a further evaluation of the dynamics of ion-pair dissociation in the closely bound CIP^{29b} relative to its freely diffusing SIP counterpart. Finally, the SIP/CIP differentiation is sharply revealed in the *nucleophilic behavior* of the quinone anion-radical moiety toward the parent quinone acceptor in eq 5, in which only the unencumbered SIP participates, the bound CIP being comparatively unreactive.

Experimental Section

Materials. Metallic potassium (Aldrich) was stored in a dry box and used without additional purification. Dibenzo-18-crown-6 (crown ether) and 4,7,13,16,21,24-hexaoxa-1,10-diazabicyclo[8.8.8]hexacosane ([2,2,2]cryptand) (Aldrich) were also used as received. *para*-Benzoquinone (BQ) and *p*-chloranil (CA) (Aldrich) were sublimed twice and recrystallized from ethanol and dried in vacuo. The alkyl-substituted quinones, duroquinone (DQ), 2,6-di-*tert*-butyl-*p*-benzoquinone (*m*-B₂Q), and 2,5-di-*tert*-butyl-*p*-benzoquinone (*p*-B₂Q) (Aldrich), were used as received. High-purity tetrahydrofuran from Merck was freshly distilled from sodium/benzophenone under an argon atmosphere and briefly stored over either a potassium or sodium mirror prior to use. Hexane (Merck) was successively washed with concentrated HNO₃/H₂SO₄, H₂O, NaOH, and H₂O, dried over CaCl₂ followed by distillation from sodium/benzophenone, and stored under an argon atmosphere.

Preparation of Ion-Pair Salts. The *p*-benzoquinones derivatives in Chart 1 were reduced with a potassium mirror in the presence of either [2,2,2]cryptand or crown ethers as follows. Potassium (7 mg, 0.179 mmol) was carefully cleaned mechanically in a glovebox under an argon atmosphere and placed in a well-dried Schlenk tube (50 mL). The tube was slowly heated in an oil bath in vacuo (10⁻³ Torr) until complete sublimation of the metal and mirror formation on the wall were apparent. In another Schlenk tube, a sample of the quinones (0.178 mmol) together with a stoichiometric amount of either cryptand or crown ethers was degassed in vacuo (10⁻³ Torr). (Note that single crystals of *p*-B₂Q^{•-} were also isolated as its potassium salt in the absence of crown ether, i.e., K⁺ was complexed with an anion radical and a THF solvate.) The degassed mixture was dissolved in 20–25 mL of dry THF, and the solution was transferred into the Schlenk tube

containing the metal mirror. An intense orange or brown coloration appeared immediately. The solution was allowed to stand at -50 °C for a 1–5 days until the reduction was complete as indicated by the complete disappearance of the potassium mirror. The resulting brown solution was carefully covered with a layer of dry hexane (20 mL) and placed for 2–3 days in a constant-temperature bath maintained at -60 °C. The reaction batch typically yielded 5–10 mg of well-formed crystals growing on the walls at the hexane/THF interface. The crystal of *p*-chloranil anion-radical salt Na(cryptand)⁺CA^{•-} was prepared by a similar procedure with a sodium mirror. The highly air-sensitive, brown or dark brown crystals were carefully collected and then used for the X-ray structural analysis (carried out at -100 °C under a protective cold nitrogen stream) and after dissolving in dry THF for EPR and UV–vis spectroscopic measurements. Note that the electron paramagnetic resonance measurements were performed on a Bruker ESP-300 X-band spectrometer and electronic spectroscopy was performed on either a Hewlett-Packard 8453 diode-array or a Varian Cary 5 spectrometer as described earlier.^{18,33}

X-ray Crystallography. Intensity data for X-ray crystallographic analysis were collected at -100 °C with a Bruker SMART Apex diffractometer using Mo Kα radiation (λ = 0.710 73 Å). The structures were solved by direct methods and refined by full matrix least-squares treatment.³⁴ The structural details are on deposit and can be obtained from the Cambridge Crystallographic Database. A full listing of crystal, data collection, and refinement parameters is given in Table 4.

Acknowledgment. We thank T.Y. Rosokha for the preparation of single crystals of Na(cryptand)⁺CA^{•-} and (DDQ₃)²⁻(N-Bu₄)₂ and the R. A. Welch Foundation and National Science Foundation for financial support. We thank Prof. S. F. Nelsen for providing us with a copy of the ESREXN program.^{33b}

Supporting Information Available: Crystal lattices and ORTEP diagrams of polymorph II of K(cryptand)⁺ (Figure S1);

- (33) (a) Lu, J.-M.; Rosokha, S. V.; Kochi, J. K. *J. Am. Chem. Soc.* **2003**, *125*, 12161. (b) Dynamic ESR simulations were carried out with the aid of the ESREXN computer program described by: Heinzer, J. Quantum Chemistry Program Exchange 209, as modified by Petillo, P. A. and Ismagilov, R. F. (34) (a) Sheldrick, G. M. *SADABS*, ver. 2.03; Bruker/Siemens Area Detector Absorption and Other Corrections: 2000. (b) Sheldrick, G. M. *SHELXS 97 – Program for Crystal Structure Solutions*; University of Göttingen: Germany, 1997. (c) Sheldrick, G. M. *SHELXL 97 – Program for Crystal Structure Refinement*; University of Göttingen: Germany, 1997.

K(cryptand)⁺**DQ**^{-•} (Figure S2); K(cryptand)⁺**p-B₂Q**^{-•} (Figure S3); K(cryptand)⁺**m-B₂Q**^{-•} (Figure S4); Na(cryptand)⁺**CA**^{-•} (Figure S5); UV–vis spectra of THF solutions of K(cryptand)⁺**BQ**^{-•}, K(crown-ether)⁺**B₂Q**^{-•}, and K(cryptand)⁺**p-B₂Q**^{-•} (Figure S6); UV–vis spectra of THF solutions **m-B₂Q**^{-•} and its solid-state spectrum (Figure S7); ESR spectra of K(cryptand)⁺**BQ**^{-•} in THF (Figure S8); ESR spectra of K(cryptand)⁺**m-**

B₂Q^{-•} in the presence of **m-B₂Q** in THF (Figure S9); unit cell and crystal data for the (1:1) adduct of **BQ**^{-•} anion radical (Figure S10); crystal lattices, ORTEP diagram, and crystal data for (**DDQ**)₃²⁻(NBu₄⁺)₂ (Figure S11). This material is available free of charge via the Internet at <http://pubs.acs.org>.

JA066471O